**Supporting Information**

# Monitoring the Viral Transmission of SARS-CoV-2 in Still Waterbodies Using Lanthanide-Doped Carbon Nanoparticle Based Sensor Array

Maha Alafeef,[1, 2, 3, 4‡] Ketan Dighe,[1,4,‡] Parikshit Moitra[2] and Dipanjan Pan[1,2,4]*

[1]Bioengineering Department, the University of Illinois at Urbana-Champaign, Urbana, 61801, USA

[2]Departments of Diagnostic Radiology and Nuclear Medicine and Pediatrics, Center for Blood Oxygen Transport and Hemostasis, University of Maryland Baltimore School of Medicine, Health Sciences Research Facility III, 670 W Baltimore St., Baltimore, Maryland 21201, United States

[3]Biomedical Engineering Department, Jordan University of Science and Technology, Irbid, Jordan

[4]Department of Chemical, Biochemical and Environmental Engineering, University of Maryland Baltimore County, Interdisciplinary Health Sciences Facility, 1000 Hilltop Circle, Baltimore, Maryland 21250, United States

The supporting information contain 19 pages, with 12 Figures and 4 Tables.

MATERIALS AND METHODS.

**Chemical reagents and solutions.**

All chemicals including tannic acid, polyethyleneimine (PEI), $PrCl_3$, $GdCl_3$, and agarose were purchased from Sigma-Aldrich and used without any further purification. $YbCl_3$ was purchased from Alfa Aesar chemicals. Brain heart infusion (BHI), Luria broth (LB), and Soy broth were purchased from Hardy Diagnostics. *E. coli*, *S. mutans*, and *B. subtilis* were procured from ATCC and the viruses were obtained from BEI Resources, NIAID, NIH. NR-52350 contains a preparation of heat-inactivated severe acute respiratory syndrome-related coronavirus 2 (SARS-CoV-2), isolate USA-WA1/2020 (BEI Resources NR-52286) diluted into Homo sapiens lung carcinoma cells (A549; ATCC ® CCL-185™), whereas NR-49452 is a preparation of influenza A virus, A/Mexico/UTMB/1/2009 (H1N1)pdm09.

**Nanoparticles Characterization.**

To visualize the CNPs morphology, TEM micrographs were obtained using a JEOL 2100 Cryo TEM instrument (Tokyo, Japan) equipped with a Gatan UltraScan 2k × 2k charge-coupled device (CCD) camera. Prior to the imaging, the samples were probe sonicated, and then 5 μL sample was drop-cast onto a holey carbon-coated copper grid. The anhydrous diameter was determined from 30 random measurements of the NPs using ImageJ software (NIH, Bethesda, MD, USA). The number-averaged hydrodynamic size and electrophoretic potential of the CNPs dispersed in water were recorded using a Malvern Zetasizer Nano series (Malvern Instruments Ltd., United Kingdom) at 25 °C based on Smoluchowski equation. The absorbance spectra of LnCNPs were recorded on a GENESYS 10 UV−Vis spectrometer (Thermo Scientific, MA). Fluorescence spectra were recorded using an Infinite 200 PRO multimode microplate reader (Tecan, NC, US).

**FT-IR Measurement.**

MirrIR IR-reflective glass slides (Kevley Technologies, Chesterland, Ohio, USA) were used for sample deposition. An aqueous suspension of the LnCNPs was dried onto the glass slides and then the measurement was taken place using Nicolet Nexus 670 FTI-IR (Fredrick Seitz Material Research Laboratories, Urbana, Illinois, USA). The measurement was collected at 1 $cm^{-1}$ spectral resolution with 200 scans per pixel for 100 × 100 μm images with a 25 × 25 μm pixel size. Separate spectra were corrected for atmospheric contributions.

**Preparation of Bacteria Solution for Selectivity Study**.

A single colony of bacteria on a solid agar plate was transferred to 10 mL corresponding broth medium and grown at 37 °C for 6-8 h (culture medium: LB for *E. coli*, BHI for *S. mutans*, and TSB for *B. subtilis*. Microorganisms were harvested by centrifuging at 4400 rpm for 5 min. The obtained microorganisms were resuspended with PBS. Then the bacterial samples were diluted to obtain various cell densities.

**Docking Studies.**

The chemical structures were first energy minimized using a general ab initio quantum chemistry package, General Atomic and Molecular Electronic Structure System (GAMESS) program. We used B3LYP functional while performing the density functional theoretical (DFT) calculations with 3-21G(d) as the basis set. Pople N31 was used for the polar groups. These energy minimized structures were then undertaken for docking studies using AutoDock 4.0 software.

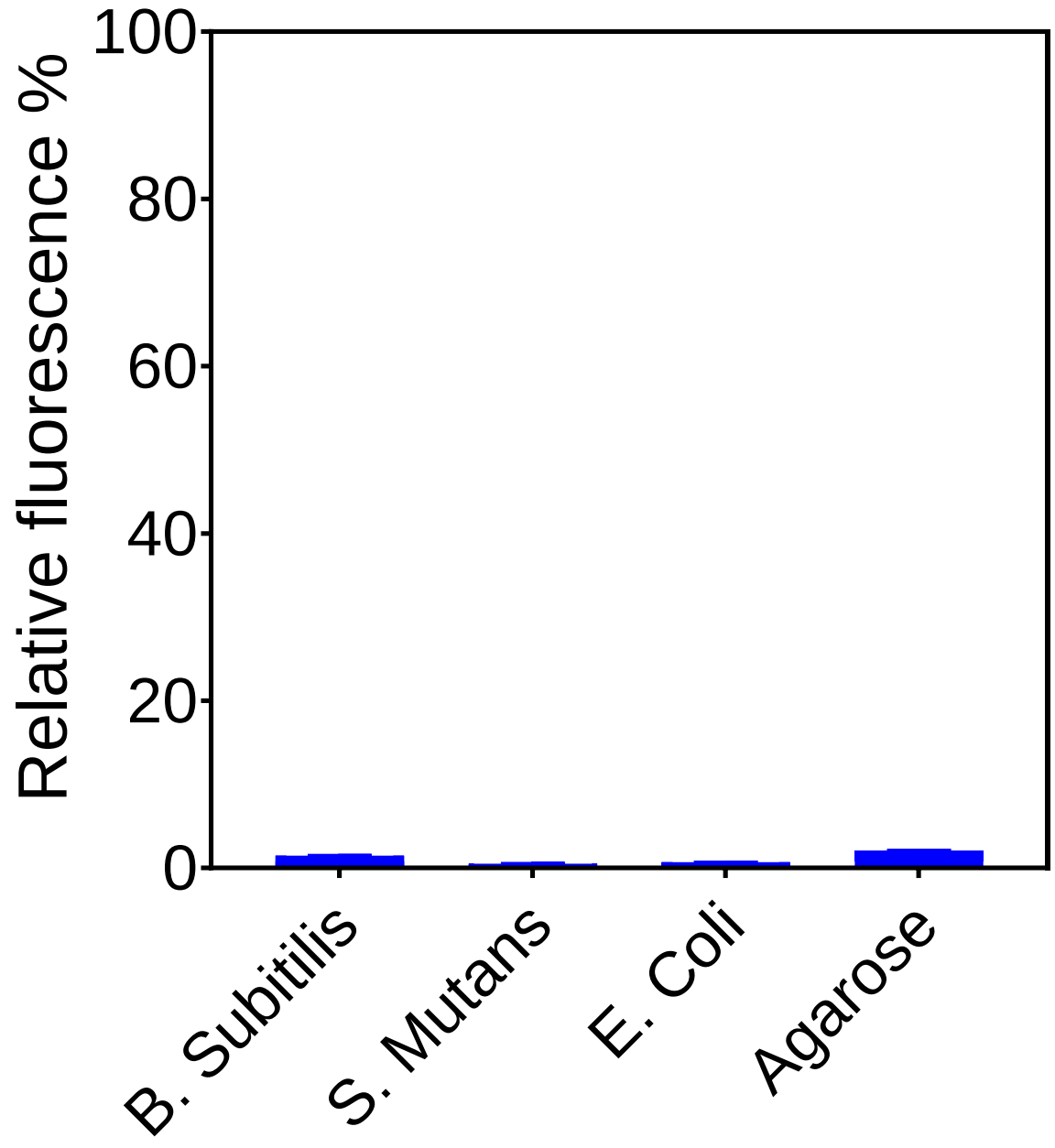


**Figure S1.** The autofluorescence of the bare agarose gel, and the bacteria cells (*B. subitilis*, *S. mutans*, and *E. coli*) relative to the LnCNPs sensor response.

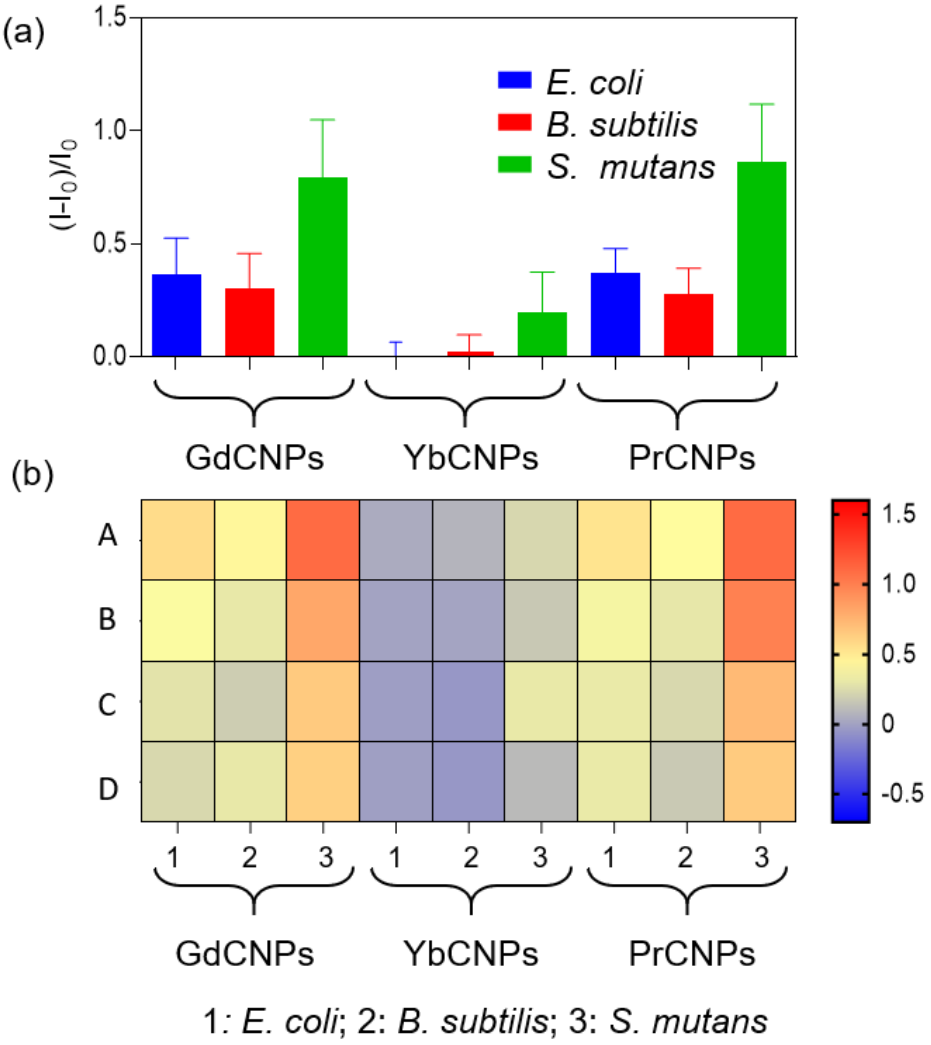


**Figure S2.** The fluorescence signature of each bacterium was recorded by the three LnCNPs-based sensor platforms. (a) Relative fluorescence intensity of the three LnCNPs was recorded for the three bacterial samples. (b) Heat map of the sensor array fluorescence response.

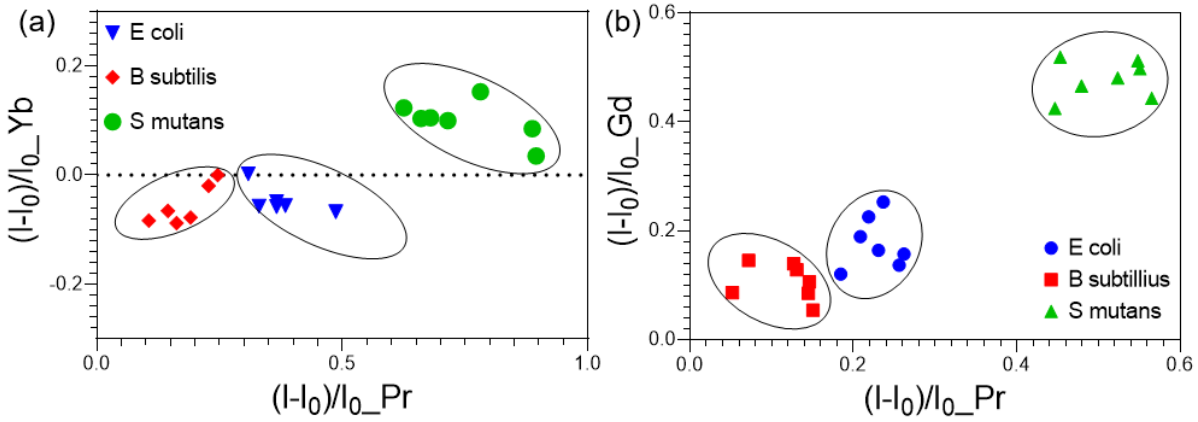


**Figure S3.** (a) 2D plot of the fluorescence output of PrCNPs vs. YbCNPs and (b) 2D plot of the fluorescence output of PrCNPs vs GdCNPs for the three bacteria.

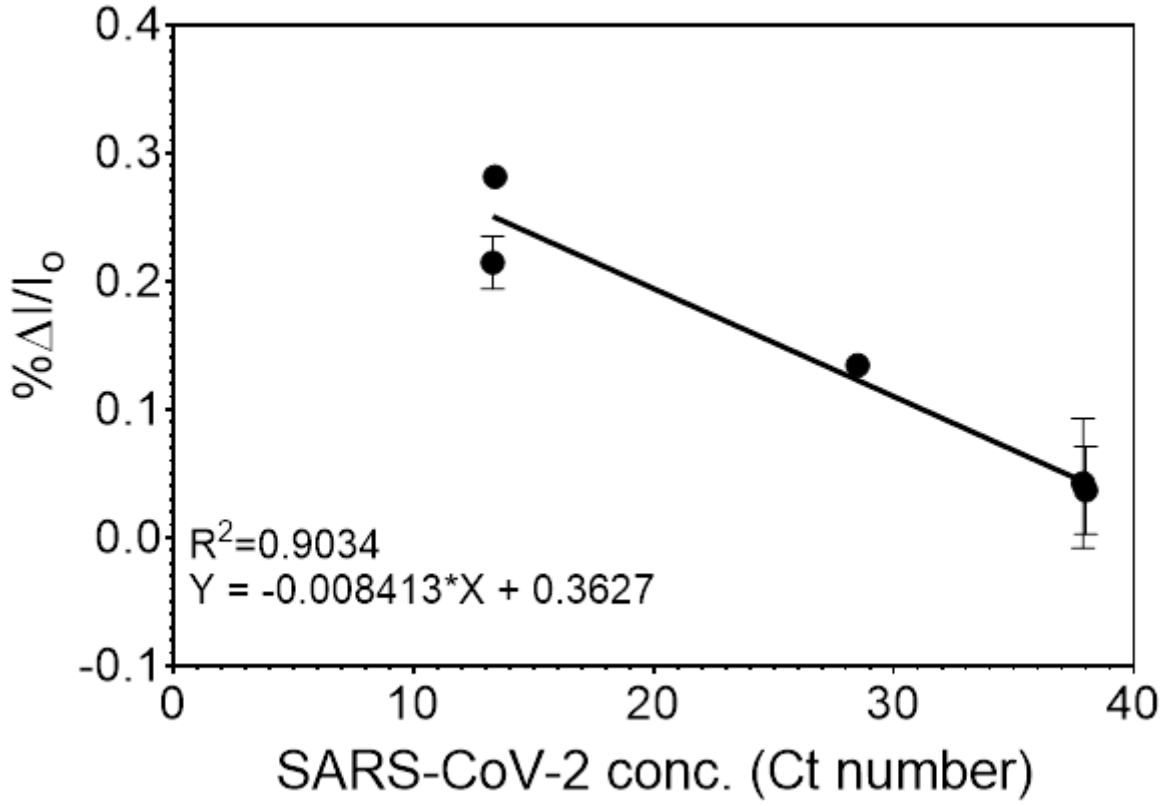


**Figure S4.** The Standard curve of the change in YbCNPs fluorescence as a function of the SARS-CoV-2 concentration (Ct numbers) obtained from RT-PCR. The fitted data was further used to evaluate the sensor array sensitivity towards SARS-CoV-2 and calculate the LOD in copies/µL.

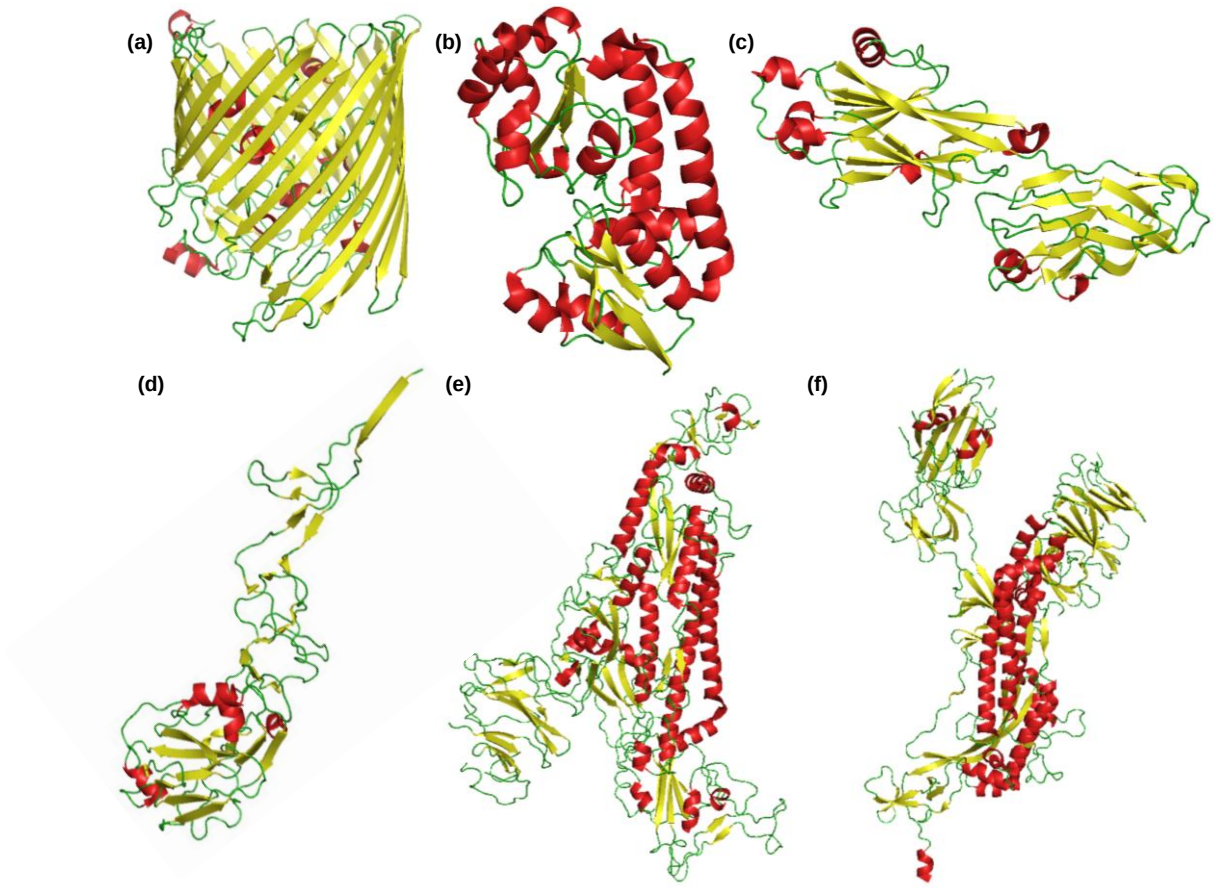


**Figure S5.** (a) Transmembrane Beta-Barrel Protein: Ferric citrate transporter FecA for *Escherichia coli* (PDB ID: 1PO3); (b) Transport Protein: triscatecholate siderophore binding protein FeuA for *B. subtilis* (PDB ID: 2WHY); (c) Cell Adhesion Protein: C-terminal domain of *S. mutans* surface protein SpaP (PDB ID: 3OPU); (d) Viral Protein: Hemagglutinin structure of an avian H1N1 influenza A virus (PDB ID: 3HTO); (e) Viral Protein: SARS-CoV spike glycoprotein (PDB ID: 5XLR); (f) Viral protein: SARS-CoV-2 spike glycoprotein (PDB ID: 6VXX).

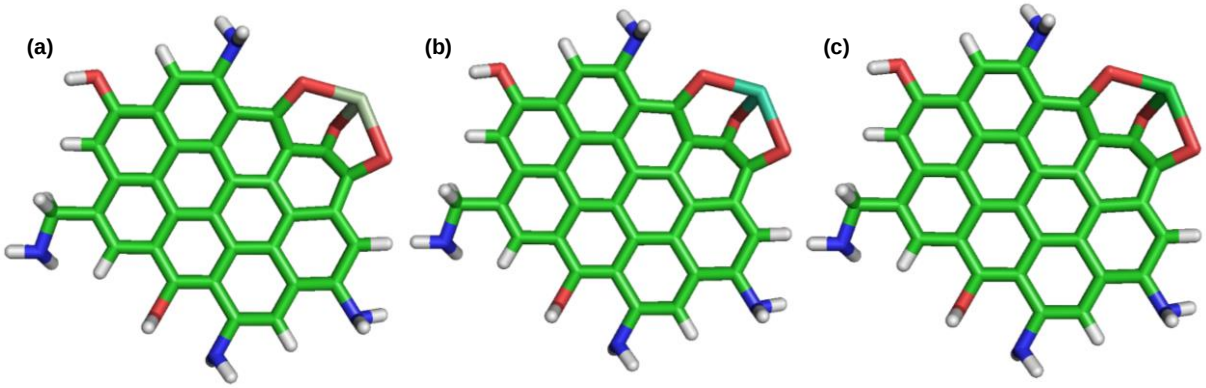


**Figure S6.** Energy minimized structures of the lanthanide-doped carbon nanoparticles: (a) PrCNPs; (b) GdCNPs and (c) YbCNPs.

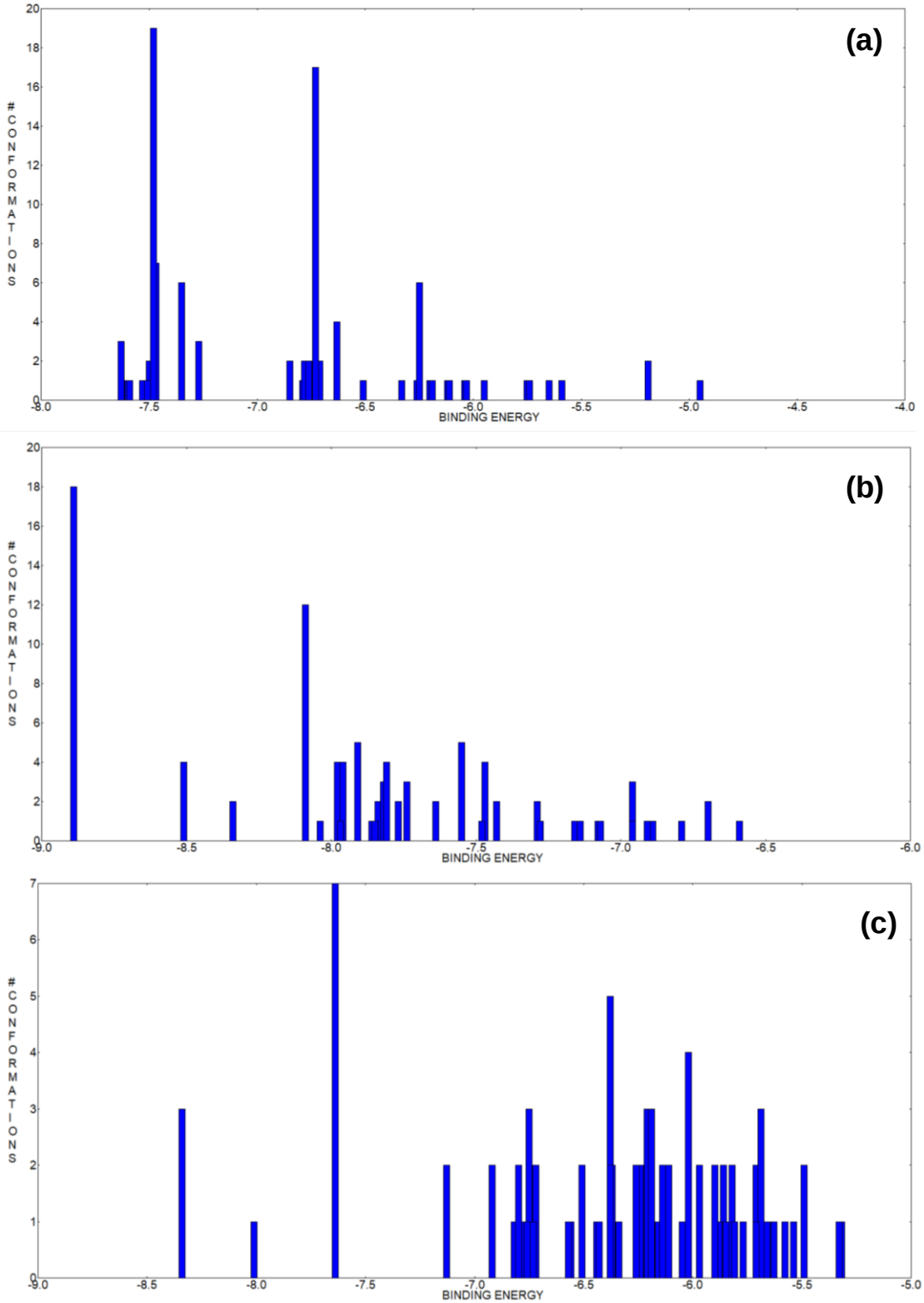


**Figure S7.** Histogram representing the number of conformations with the binding energy for (a) 1PO3 (*E. coli*) : GdCNP; (b) 2WHY (*B. subtilis*) : GdCNP and (c) 3OPU (*S. mutans*) : PrCNP protein-ligand complexes.

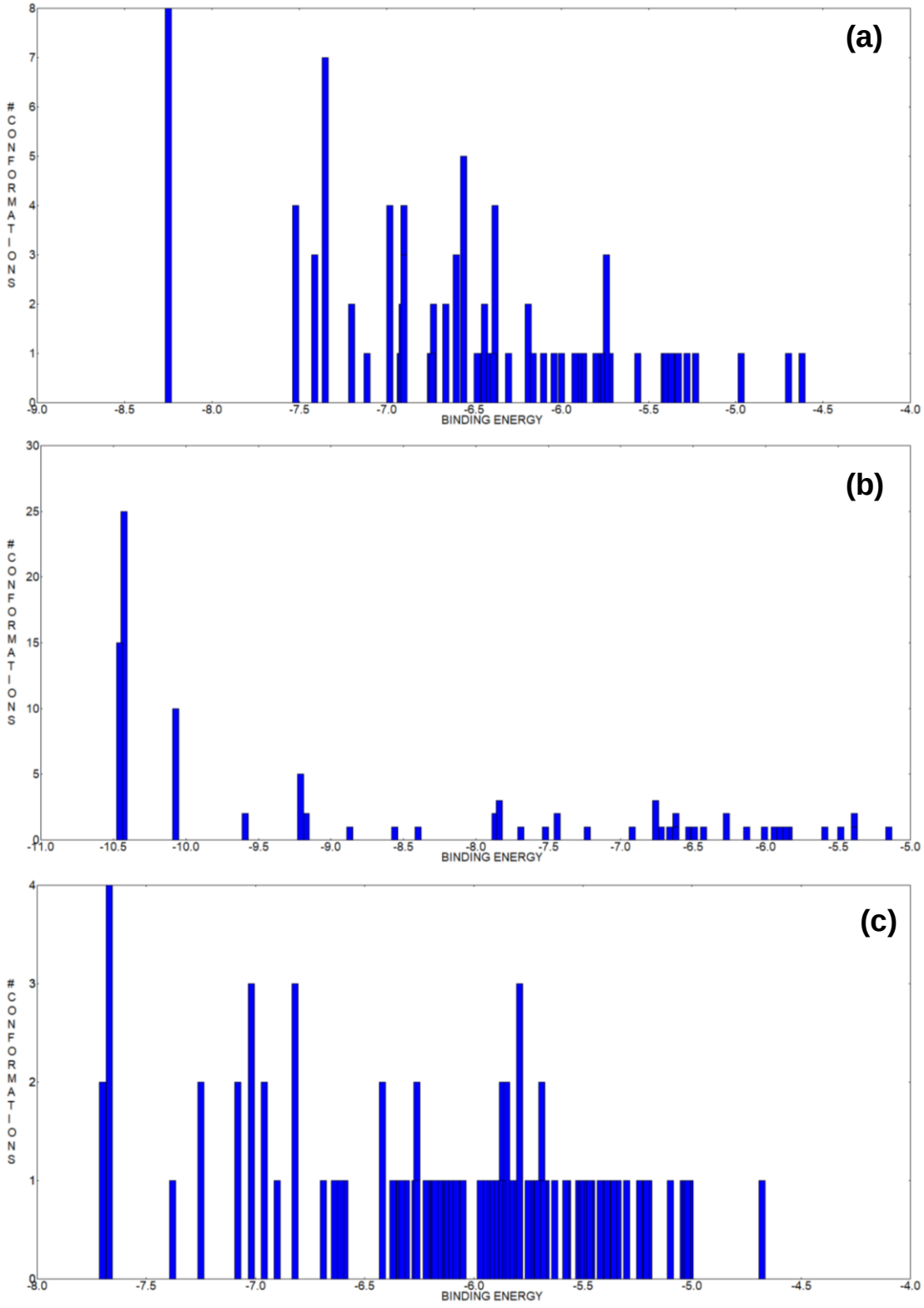


**Figure S8.** Histogram representing the number of conformations with the binding energy for (a) 3HTO (H1N1 influenza A) : PrCNP; (b) 5XLR (SARS-CoV) : PrCNP and (c) 6VXX (SARS-CoV-2) : GdCNP protein-ligand complexes.

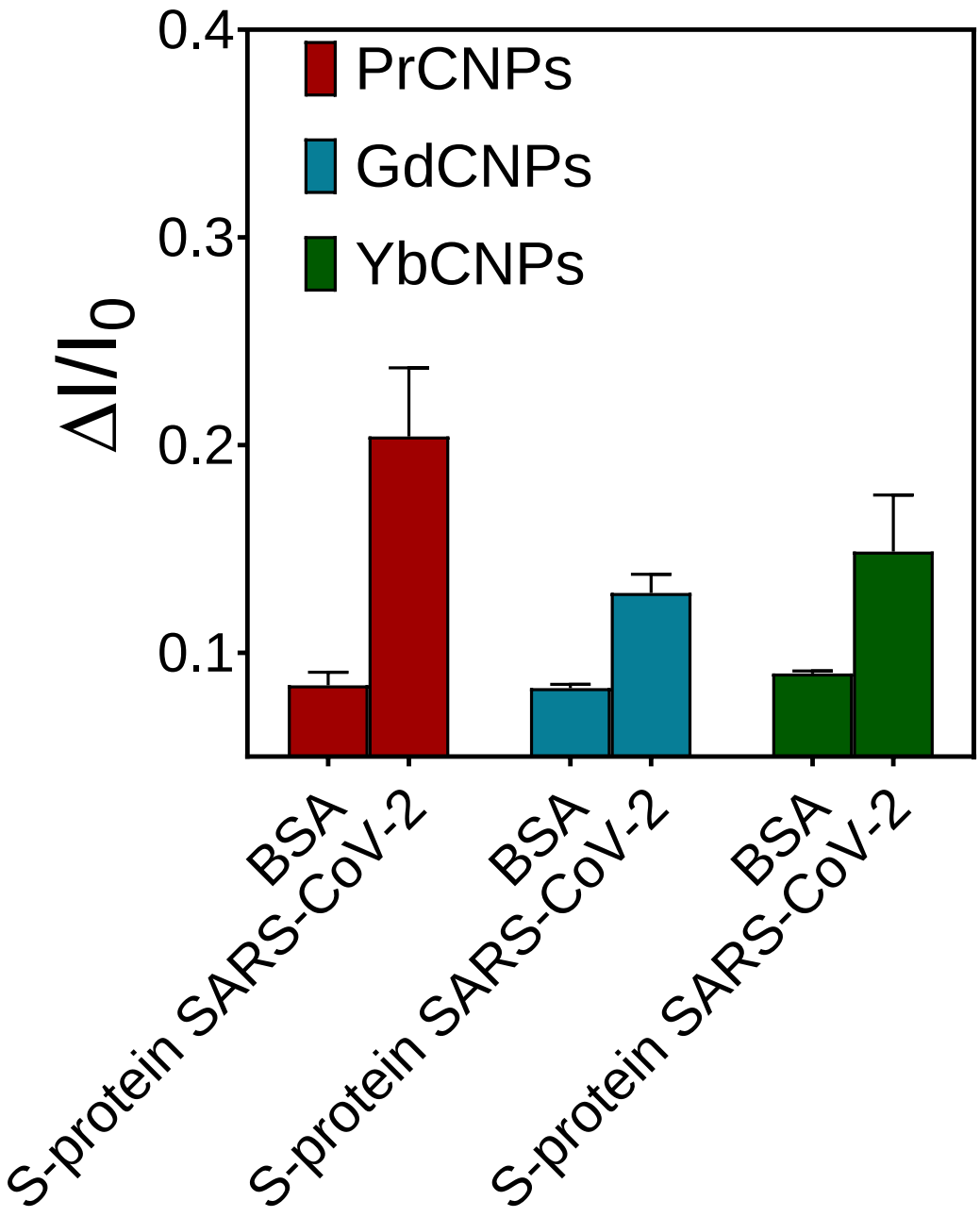


**Figure S9.** The LnCNPs sensor response towards the bovine serum albumin (BSA) and SARS-CoV-2 spike protein. The BSA shows a very low response when compared to an equivalent amount of the SARS-CoV-2 spike protein.

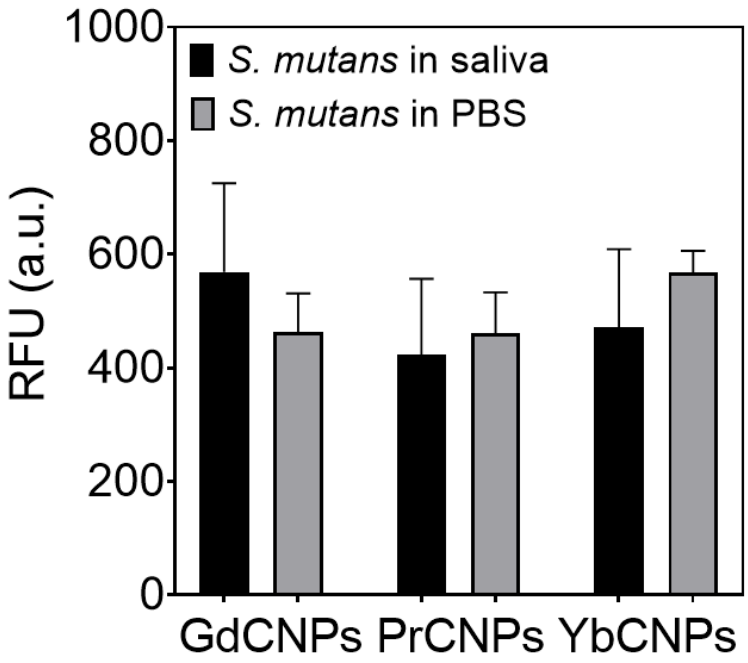


**Figure S10.** Fluorescence response of LnCNPs sensor array toward *S. mutans* in both artificial saliva and PBS.

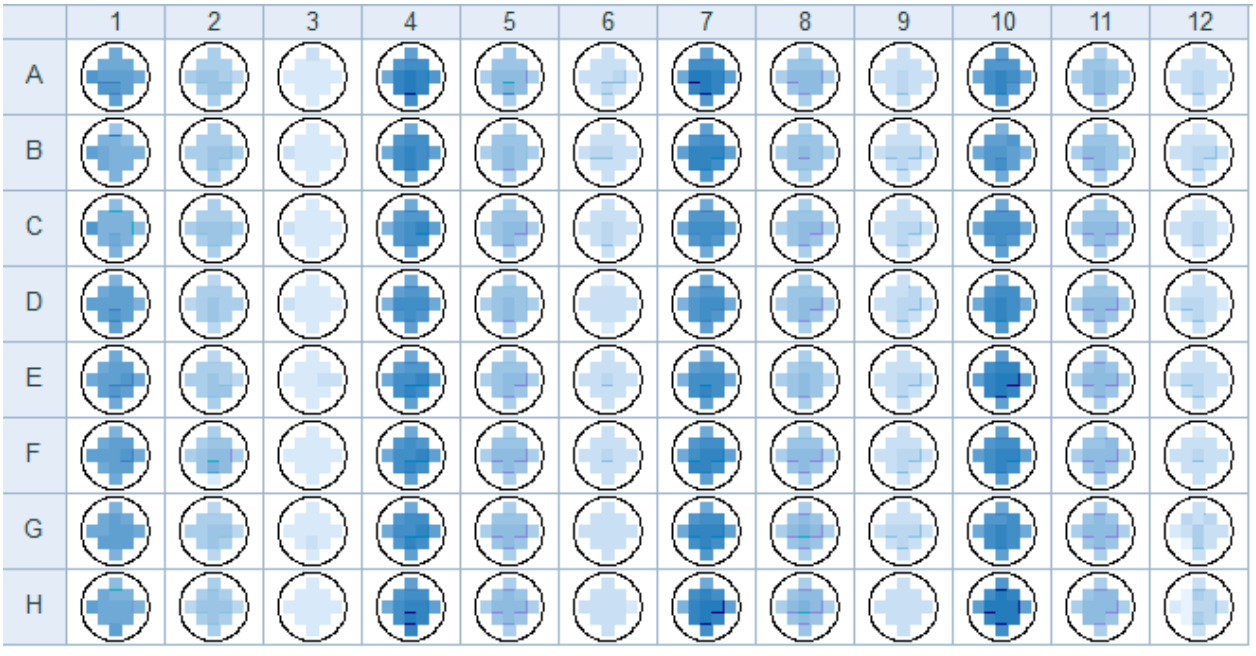


**Figure S11.** The fluorescence intensity scan of the 96-well plate LnCNPs sensor array, $\lambda_{Ex}$=360nm and $\lambda_{Em}$=460nm.

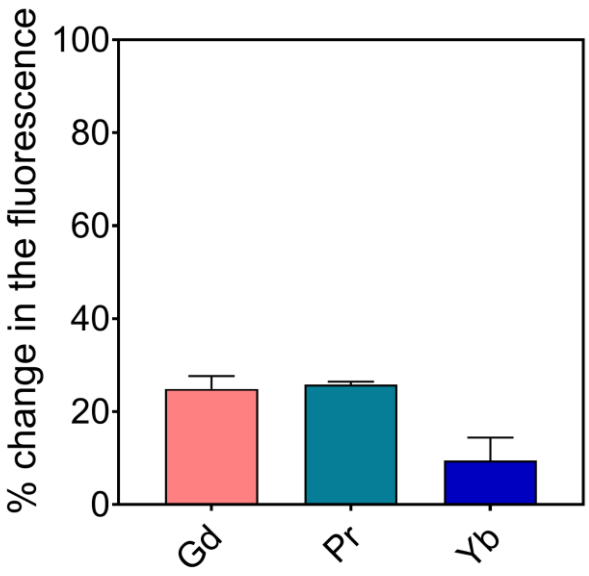


**Figure S12.** The stability data of the LnCNPs sensor array. A relative change in the fluorescence signal of less than 25% was observed after a month of fabricating the sensor array. The sensor was stored at room temperature away from light.

**Table S1.** LnCNPs sensor array response to *E. coli* samples with cell density ranging from 1-$10^7$ cells. The sensor provides a distinct and detectable response up to single-cell resolution.

| | **GdNPs** | | **PrCNPs** | | **YbCNPs** | |
|---|---|---|---|---|---|---|
| | Mean | SD | Mean | SD | Mean | SD |
| **$10^7$** | 0.63 | 0.10 | 0.54 | 0.10 | 0.62 | 0.02 |
| **$10^6$** | 0.58 | 0.02 | 0.46 | 0.01 | 0.63 | 0.01 |
| **$10^5$** | 0.31 | 0.3 | 0.31 | 0.18 | 0.45 | 0.24 |
| **$10^4$** | 0.17 | 0.06 | 0.04 | 0.01 | 0.024 | 0.01 |
| **$10^3$** | 0.14 | 0.05 | 0.06 | 0.007 | 0.24 | 0.009 |
| **$10^2$** | 0.09 | 0.07 | 0.10 | 0.04 | 0.07 | 0.01 |
| **10** | 0.01 | 0.01 | 0.10 | 0.04 | 0.20 | 0.08 |
| **1** | 0.19 | 0.01 | 0.09 | 0.12 | 0.15 | 0.07 |

**Table S2.** Comparative free energies of binding and clustering efficiencies of lanthanide-doped carbon nanoparticles and surface proteins of bacteria and viruses.

| Protein | LnCNPs | Average Free Energy of Binding (kcal/mol) | Clustering |
|---|---|---|---|
| **1PO3 (E. coli)** | **Gd** | **-7.38** | **37/100** |
| 1PO3 (E. coli) | Pr | -7.24 | 43/100 |
| 1PO3 (E. coli) | Yb | -6.02 | 38/100 |
| **2WHY (B. subtilis)** | **Gd** | **-7.85** | **35/100** |
| 2WHY (B. subtilis) | Pr | -6.95 | 37/100 |
| 2WHY (B. subtilis) | Yb | -7.90 | 36/100 |
| 3OPU (S. mutans) | Gd | -5.71 | 63/100 |
| **3OPU (S. mutans)** | **Pr** | **-7.41** | **57/100** |
| 3OPU (S. mutans) | Yb | -6.02 | 65/100 |
| 3HTO (H1N1 influenza A) | Gd | -7.33 | 50/100 |
| **3HTO (H1N1 influenza A)** | **Pr** | **-7.46** | **54/100** |
| 3HTO (H1N1 influenza A) | Yb | -7.28 | 52/100 |
| 5XLR (SARS-CoV) | Gd | -6.21 | 38/100 |
| **5XLR (SARS-CoV)** | **Pr** | **-7.69** | **38/100** |
| 5XLR (SARS-CoV) | Yb | -7.89 | 47/100 |
| **6VXX (SARS-CoV-2)** | **Gd** | **-6.18** | **82/100** |
| 6VXX (SARS-CoV-2) | Pr | -5.55 | 73/100 |
| 6VXX (SARS-CoV-2) | Yb | -5.93 | 68/100 |

**Table S3.** List of participating amino acids and functional groups from lanthanide-doped carbon nanoparticles in the respective protein-ligand complexes.

| Protein-ligand complex | Participating functional groups from LnCNPs | Interacting amino acids |
|---|---|---|
| 1PO3 (E. coli) : GdCNP | 2 –OH and 2 –$NH_2$ | ASP-305 (-OH), ASN-381 (-OH), TYR-368 (-$NH_2$), GLU-307 (-$NH_2$) |
| 2WHY (B. subtilis) : GdCNP | 2 –OH and 3 –$NH_2$ | GLN-215 (-OH), GLU-216 (-OH), GLU-216 (–$NH_2$), TYR-185 (–$NH_2$), GLN-181 (–$NH_2$) |
| 3OPU (S. mutans) : PrCNP | 6 –OH and 4 -$NH_2$ | ALA-1424 (-OH), THR-1422 (-OH), TYR-1421 (-OH), GLN-1420 (-OH), GLN-1395 (-OH), GLY-1394 (-OH), TYR-1396 (-$NH_2$), GLN-1395 (-$NH_2$), GLY-1394 (-$NH_2$), TYR-1392 (-$NH_2$) |
| 3HTO (H1N1) : PrCNP | 3 –OH and 4 –$NH_2$ | THR-302 (-OH), SER-266 (-OH), ASP-265 (-OH), PRO-300 (-$NH_2$), SER-266 (-$NH_2$), ASP-265 (-$NH_2$), GLU-107 (-$NH_2$) |
| 5XLR (SARS-CoV) : PrCNP | 3 –OH and 4 -$NH_2$ | THR-559 (-OH), THR-559 (-OH), ASP-572 (-OH), ILE-573 (-$NH_2$), ASP-560 (-$NH_2$), THR-559 (-$NH_2$), THR-533 (-$NH_2$) |
| 6VXX (SARS-CoV-2) : GdCNP | 3 –OH and 4 -$NH_2$ | PRO-1069 (-OH), ARG-1107 (-OH), ILE-714 (-OH), GLU-1072 (-$NH_2$), GLU-1072 (-$NH_2$), TYR-1047 (-$NH_2$), SER-711 (-$NH_2$) |

**Table S4.** The performance characteristics of previously reported biosensors.

| Detection Approach | Type of Nanoparticle | Pathogen Model | Detection Limit | Fluid | Reference |
|---|---|---|---|---|---|
| Electrochemical | Gold Nanoparticle | *S. typhi* | 98.9 cfu/mL | PBS | 1 |
| Fluorescence | Quantum Dot | *S. typhi* | $10^3$ cells/mL | | 2 |
| Fluorescence | Quantum Dot | *E. coli O157:H7* | $10^6$ cells/mL | PBS | 3 |
| Fluorescence | Quantum Dot | *C. parvum; G. lamblia* | not reported | PBS | 4 |
| Fluorescence | Quantum Dot | *Lysteria monocytogenes* | not reported | PBS | 5 |
| Fluorescence | Quantum Dot | *B. thuringiensis* | $10^3$-$10^4$ cfu | PBS | 6 |
| Fluorescence | Quantum Dot | *E. coli* | Not reported | | 7 |
| Colorimetric | Gold Nanoparticles | *E. coli (XL1)* | $1 \times 10^2$ bacteria/mL | | 8 |
| Colorimetric | MNPs | *E. coli O157:H7; E. coli* BL 21 | 5 cfu/mL; 20 cfu/mL | | 9 |
| Colorimetric | Gold Nanoparticles | *E. coli O157:H7* | 1.8 cfu/mL | | 10 |
| Colorimetric | MNPs and $TiO_2$ nanocrystals | *Salmonella* | >100 cfu/mL | | 11 |
| Colorimetric | MNPs | *E. coli; Sarcina lutea; Proteus vulgaris* | N. A | | 12 |
| Colorimetric | Citrate-capped Au NPs and Ag NPs with different sizes | *Bacteria: CRPA, Acetobacter aceti, Rhodopseudomonas, Bacillus natto, Staphylococcus, E. coli, Bacillus* | | | 13 |
| Colorimetric and Luminescence | Au NPs stabilized by GQDs | *Microorganisms: E. coli O157:H7, E. coli ATCC35218, P. aeruginosa CICC10204, P. aeruginosa CICC21954, B. subtilis CICC10071, B. subtilis CICC10275* | | | 14 |

| | | | | | |
|---|---|---|---|---|---|
| Fluorescence | RuBpy doped silica | *Mycobacterium spp.* | $10^5$ cells/mL | Urine | 15 |
| Fluorescence | Gold nanorod | *Toxoplasma gondii Tachyzoites* | Not reported | Cell culture Medium | 16 |
| Fluorescence | Gold nanorod | *Pseudomonas aeruginosa* | Not reported | 0.85% sodium chloride | 17 |
| Fluorescence | Gold/silicon nanorod | *S. typhi; RSV* | Not reported | | 18 |
| Fluorescence | Magnetic bead/quantum dot | *E. coli 0157:H7* | $10^3$ and $10^4$ cfu/mL | brain heart infusion broth | 19-20 |
| Fluorescence | Magnetic nanoparticle | *Mycobacterium spp.* | ~250 cells/mL | | 21 |
| Fluorescence | Magnetic nanoparticle | *E. coli* | Not reported | | 22 |
| SERS | Silver Nanoshell | *E. coli* | 3-5 cells (water) | Water | 23 |
| SERS | Gold Nanoparticle | *Mycobacterium avium subspecies Paratuberculosis* | $10^3$ cells/mL (milk) | Milk | 24 |
| SERS | Gold Nanoparticle | *Feline Calcivirus* | $10^6$ pfu/mL (urine) | Urine | 25 |
| SERS | Gold Nanoparticle | *Cryptosporidium parvum Giardia lamblia* | Not reported | | 26 |
| SERS | Gold Nanoparticle | *E. coli; MS2 bacteriophage; PRD1 bacteriophage* | $10^6$ cells/mL NR $10^9$ pfu/mL | | 27 |
| SERS | Silver Nanoparticle | *Rhodococcus rhodochrous E. coli* | Not reported | | 28 |
| SERS | Silver Nanoparticle | *E. coli, B. subtilis S. aureus* | Not reported | | 29-30 |
| SPR | Silver Nanoshell | *E. coli* | 3-5 cells | Water | 31 |
| Magnetic | Magnetic nanoparticle | *Mycobacterium avium spp. Paratuberculosis* | 15.5 cfus | Milk | 32 |
| Magnetic | Magnetic nanoparticle | *E. coli O157:H7* | 104 cfu/mL | TWEEN/ PBS | 33 |

| | | | | | |
|---|---|---|---|---|---|
| Magnetic | Magnetic nanoparticle | *E. coli* | Not reported | | 34 |
| Magnetic | Magnetic nanoparticle | *S. aureus; S. epidermidis* | 8 cfu/mL | | 35-39 |
| Magnetic | Magnetic nanoparticle | *E. coli; E. faecalis; S. aureus; S. epidermidis* | 10 cfu/mL (not reported); not reported | MES buffer | 40 |
| Colorimetric | Gold | SARS | 60 fmol | | 41 |
| Electrochemical | Gold | SARS | 2.5 pM | | 42 |
| Fluorometric | Gold | H1N1 (Influenza) | 13.9 pg/mL | | 43 |
| SERS | Gold | H1N1 (Influenza) | 25nM | | 44 |
| Fluorometric | Gold | H1N1 (Influenza) | 25nM | | 44 |
| Electrochemical | Gold | H1N1 (Influenza) | 577 pM | | 45 |
| Colorimetric | Gold | H1N1 (Influenza) | 1pg | | 46 |
| Colorimetric | Gold | H5N1 | 40 – 0.1 ng | | 47 |
| Electrochemical | Gold | H5N1 | 0.4 pM | | 48 |
| Fluorometric | Gold | H5N1 | 0.09 ng/mL | | 49 |
| Colorimetric | Gold | H5N1 | 10 ng/mL | | 50 |
| Electrical | Gold | HPV | 30 pM | | 51 |
| Fluorometric | Gold | HPV | 1 fM | | 52 |
| Colorimetric | Gold | HIV | ~11 $\log_{10}$ copies/mL | | 53 |
| Electrochemical | Gold | HIV | 0.34 fM | | 54 |

**References**


1. Dungchai, W.; Siangproh, W.; Chaicumpa, W.; Tongtawe, P.; Chailapakul, O. *Salmonella typhi* determination using voltammetric amplification of nanoparticles: A highly sensitive strategy for metalloimmunoassay based on a copper-enhanced gold label. *Talanta* **2008**, *77*, 727–732.
2. Yang, L. J.; Li, Y. B. Quantum dots as fluorescent labels for quantitative detection of Salmonella typhimurium in chicken carcass wash water. *J. Food Prot.* **2005**, 68, 1241–1245.
3. Hahn, M. A.; Keng, P. C.; Krauss, T. D. Flow cytometric analysis to detect pathogens in bacterial cell mixtures using semiconductor quantum dots. *Anal. Chem.* **2008**, 80, 864–872.
4. Zhu, L.; Ang, S.; Liu, W. T. Quantum dots as a novel immunofluorescent detection system for Cryptosporidium parvum and Giardia lamblia. Appl. Environ. Microbiol. 2004, 70, 597–598.
5. Tully, E.; Hearty, S.; Leonard, P.; O'Kennedy, R. The development of rapid fluorescence-based immunoassays, using quantum dot-labelled antibodies for the detection of Listeria monocytogenes cell surface proteins. *Int. J. Biol. Macromol.* **2006**, 39, 127–134.
6. Ikanovic, M.; Rudzinski, W. E.; Bruno, J. G.; Allman, A.; Carrillo, M. P.; Dwarakanath, S.; Bhahdigadi, S.; Rao, P.; Kiel, J. L.; Andrews, C. J. Fluorescence assay based on aptamer-quantum dot binding to Bacillus thuringiensis spores. *J. Fluoresc.* **2007**, 17, 193–199.
7. Leevy, W. M.; Lambert, T. N.; Johnson, J. R.; Morris, J.; Smith, B. D. Quantum dot probes for bacteria distinguish Escherichia coli mutants and permit in vivo imaging. *Chem. Commun.* **2008**, 2331–2333.
8. Miranda, O.R.; Li, X.; Garcia-Gonzalez, L.; Zhu, Z.-J.; Yan, B.; Bunz, U.H.; Rotello, V.M. Colorimetric Bacteria Sensing Using a Supramolecular Enzyme-Nanoparticle Biosensor. *J. Am. Chem. Soc*. **2011**, 133, 9650–9653.
9. Hossain, S.Z.; Ozimok, C.; Sicard, C.; Aguirre, S.D.; Ali, M.M.; Li, Y.; Brennan, J.D. Multiplexed paper test strip for quantitative bacterial detection. Anal. Bioanal. Chem. 2012, 403, 1567–1576.
10. Jung, B.Y.; Jung, S.C.; Kweon, C.H. Development of a rapid immunochromatographic strip for detection of Escherichia coli O157. *J. Food Prot.* **2005**, 68, 2140–2143.
11. Joo, J.; Yim, C.; Kwon, D.; Lee, J.; Shin, H.H.; Cha, H.J.; Jeon, S. A facile and sensitive detection of pathogenic bacteria using magnetic nanoparticles and optical nanocrystal probes. *Analyst* **2012**, 137, 3609–3612.
12. Huang, Y.-F.; Wang, Y.-F.; Yan, X.-P. Amine-Functionalized Magnetic Nanoparticles for Rapid Capture and Removal of Bacterial Pathogens. Environ. Sci. Technol. 2010, 44, 7908–7913.
13. D. Li, Y. Dong, B. Li, Y. Wu, K. Wang and S. Zhang, *Analyst*, **2015**, 140, 7672–7677.

14. X. Lin, X. Hai, N. Wang, X.-W. Chen and J.-H. Wang, Anal. Chim. Acta, 2017, 992, 105–111.
15. Qin, D. L.; He, X. X.; Wang, K. M.; Tan, W. H. Using fluorescent nanoparticles and SYBR Green I based two-color flow cytometry to determine Mycobacterium tuberculosis avoiding false positives. *Biosens. Bioelect.* **2008**, 24, 626–631.
16. Pissuwan, D.; Valenzuela, S. M.; Miller, C. M.; Cortie, M. B. A golden bullet? Selective targeting of toxoplasma gondii tachyzoites using anti body-functionalized gold nanorods. *Nano Lett.* **2007**, 7, 3808–3812.
17. Norman, R. S.; Stone, J. W.; Gole, A.; Murphy, C. J.; Sabo- Attwood, T. L. Targeted photothermal lysis of the pathogenic bacteria Pseudomonas aeruginosa, with gold nanorods. *Nano Lett.* **2008**, 8, 302–306.
18. Fu, J.; Park, B.; Siragusa, G.; Jones, L.; Tripp, R.; Zhao, Y. P.; Cho, Y. J. An Au/Si hetero-nanorod-based biosensor for Salmonella detection. *Nanotechnology* **2008**, 19.
19. Yang, L. J.; Li, Y. B. Simultaneous detection of Escherichia coli O157:H7 and Salmonella Typhimurium using quantum dots as fluorescence labels. *Analyst* **2006**, 131, 394–401.
20. Su, X. L.; Li, Y. B. Quantum dot biolabeling coupled with immunomagnetic separation for detection of Escherichia coli O157:H7. *Anal. Chem.* **2004**, 76, 4806–4810.
21. Chang, S. C.; Adriaens, P. Nano-immunodetection and quantification of mycobacteria in metalworking fluids. *Environ. Eng. Sci.* **2007**, 24, 58–72.
22. El-Boubbou, K.; Gruden, C.; Huang, X. Magnetic glyconanoparticles: A unique tool for rapid pathogen detection, decontamination, and strain differentiation. *J. Am. Chem. Soc.* **2007**, 129, 13392–13393.
23. Kalele, S. A.; Kundu, A. A.; Gosavi, S. W.; Deobagkar, D. N.; Deobagkar, D. D.; Kulkarni, S. K. Rapid detection of Escherichia coli by using anti body-conjugated silver nanoshells. *Small* **2006**, 2, 335–338.
24. Yakes, B. J.; Lipert, R. J.; Bannantine, J. P.; Porter,M.D. Detection of Mycobacterium avium subsp paratuberculosis by a sonicate immunoassay based on surface-enhanced Raman scattering. *Clin. Vaccine Immunol.* **2008**, 15, 227–234.
25. Driskell, J. D.; Kwarta, K. M.; Lipert, R. J.; Porter, M. D.; Neill, J. D.; Ridpath, J. F. Low-level detection of viral pathogens by a surface-enhanced Raman scattering based immunoassay. *Anal. Chem.* **2005**, 77, 6147–6154.
26. Rule, K. L.; Vikesland, P. J. Surface-enhanced resonance Raman spectroscopy for the rapid detection of Cryptosporidium parvum and Giardia lamblia. *Environ. Sci. Technol.* **2009**, 43, 1147–1152.
27. Goeller, L. J.; Riley, M. R. Discrimination of bacteria and bacteriophages by Raman spectroscopy and surface-enhanced Raman spectroscopy. *Appl. Spectrosc.* **2007**, 61, 679–685.
28. Naja, G.; Bouvrette, P.; Hrapovic, S.; Luong, J. H. T. Raman based detection of bacteria using silver nanoparticles conjugated with antibodies. *Analyst* **2007**, 132, 679–686.
29. Jarvis, R. M.; Goodacre, R. Discrimination of bacteria using surface-enhanced Raman spectroscopy. *Anal. Chem.* **2004**, 76, 40–47.

30. Jarvis, R. M.; Brooker, A.; Goodacre, R. Surface-enhanced Raman scattering for the rapid discrimination of bacteria. *Faraday Discuss.* **2006**, 132, 281–292.
31. Kalele, S. A.; Kundu, A. A.; Gosavi, S. W.; Deobagkar, D. N.; Deobagkar, D. D.; Kulkarni, S. K. Rapid detection of Escherichia coli by using anti body-conjugated silver nanoshells. *Small* **2006**, 2, 335–338.
32. Kaittanis, C.; Naser, S. A.; Perez, J. M. One-step, nanoparticlemediated bacterial detection with magnetic relaxation. *Nano Lett.* **2007**, 7, 380–383.
33. Arcidiacono, S.; Pivarnik, P.; Mello, C. M.; Senecal, A. Cy5 labeled antimicrobial peptides for enhanced detection of Escherichia coli O157:H7. *Biosens. Bioelect.* **2008**, 23, 1721– 1727.
34. Hatch, D. M.; Weiss, A. A.; Kale, R. R.; Iyer, S. S. Biotinylated Bi- and Tetra-antennary Glycoconjugates for Escherichia coli Detection. *ChemBioChem* **2008**, 9, 2433–2442.
35. Gu, H. W.; Ho, P. L.; Tsang, K. W. T.; Wang, L.; Xu, B. Using biofunctional magnetic nanoparticles to capture vancomycinresistant enterococci and other gram-positive bacteria at ultralow concentration. *J. Am. Chem. Soc.* **2003**, 125, 15702–15703.
36. Gu, H. W.; Ho, P. L.; Tong, E.; Wang, L.; Xu, B. Presenting vancomycin on nanoparticles to enhance antimicrobial activities. *Nano Lett.* **2003**, 3, 1261–1263.
37. Gu, H. W.; Ho, P. L.; Tsang, K. W. T.; Yu, C. W.; Xu, B. Using biofunctional magnetic nanoparticles to capture Gram-negative bacteria at an ultra-low concentration. *Chem. Commun.* **2003**, 1966–1967.
38. Ge, M.; Chen, Z.; Onishi, H. R.; Kohler, J.; Silver, L. L.; Kerns, R.; Fukuzawa, S.; Thompson, C.; Kahne, D. Vancomycin derivatives that inhibit peptidoglycan biosynthesis without binding D-Ala-D-Ala. *Science* **1999**, 284, 507–511.
39. Gu, H. W.; Xu, K. M.; Xu, C. J.; Xu, B. Biofunctional magnetic nanoparticles for protein separation and pathogen detection. Chem. *Commun*. **2006**, 941–949.
40. Kell, A. J.; Somaskandan, K.; Stewart, G.; Bergeron, M. G.; Simard, B. Superparamagnetic nanoparticle-polystyrene bead conjugates as pathogen capture mimics: A parametric study of factors affecting capture efficiency and specificity. *Langmuir* **2008**, 24, 3493–3502.
41. H. Li, L. Rothberg, *Proceedings of the National Academy of Sciences of the United States of America* **2004**, 101, 14036.
42. G. Martínez-Paredes, M. B. González-García, A. Costa-García, *Electroanalysis* **2009**, 21, 379.
43. Y.-F. Chang, S.-F. Wang, J. C. Huang, L.-C. Su, L. Yao, Y.-C. Li, S.-C. Wu, Y.-M. A. Chen, J.-P. Hsieh, C. Chou, *Biosensors and Bioelectronics* **2010**, 26, 1068.
44. E.-O. Ganbold, T. Kang, K. Lee, S. Y. Lee, S.-W. Joo, *Colloids and Surfaces B: Biointerfaces* **2012**, 93, 148.
45. A. Bonanni, M. I. Pividori, M. del Valle, *Analyst* **2010**, 135, 1765.
46. H. Nikbakht, P. Gill, A. Tabarraei, A. Niazi, *RSC Advances* **2014**, 4, 13575.
47. J.-C. Wu, C.-H. Chen, J.-W. Fu, H.-C. Yang, *Sensors* **2014**, 14, 4399.
48. X. Liu, Z. Cheng, H. Fan, S. Ai, R. Han, *Electrochimica Acta* **2011**, 56, 6266.
49. X. Li, D. Lu, Z. Sheng, K. Chen, X. Guo, M. Jin, H. Han, *Talanta* **2012**, 100, 1.

50. B. Mu, X. Huang, P. Bu, J. Zhuang, Z. Cheng, J. Feng, D. Yang, C. Dong, J. Zhang, X. Yan, *Journal of Virological Methods* **2010**, 169, 282.
51. T. J. Baek, P. Y. Park, K. N. Han, H. T. Kwon, G. H. Seong, *Analytical and Bioanalytical Chemistry* **2008**, 390, 1373.
52. H. Zhang, L. Liu, C.-W. Li, H. Fu, Y. Chen, M. Yang, *Biosensors and Bioelectronics* **2011**, 29, 89.
53. B. A. Rohrman, V. Leautaud, E. Molyneux, R. R. Richards-Kortum, *PloS one* **2012**, 7, e45611.
54. Y. Hu, S. Hua, F. Li, Y. Jiang, X. Bai, D. Li, L. Niu, *Biosensors and Bioelectronics* **2011**, 26, 4355.